Limnol. Oceanogr., 51(5), 2006, 1956–1968

Boundary layer turbulence and flow structure over a fringing coral reef

Matthew A. Reidenbach[1] *and Stephen G. Monismith*[2]
Environmental Fluid Mechanics Laboratory, Stanford University, Stanford, California 94305-4020

Jeffrey R. Koseff
Environmental Fluid Mechanics Laboratory, Stanford University, Stanford, California 94305-4020

Gitai Yahel[3] *and Amatzia Genin*
The Hebrew University of Jerusalem, H. Steinitz Marine Biological Laboratory, The Interuniversity Institute for Marine Sciences, P.O. Box 469, Eilat 88103, Israel

Abstract

Measurements of velocity and rates of turbulence were made across a fringing coral reef in the Gulf of Aqaba, Red Sea, to determine the effect that the rough topography has on boundary layer mixing and flow dynamics. Observations were made at two fore-reef sites and a nearby sandy slope. The friction velocity, u_*, and drag coefficient, C_D, were determined directly from turbulent Reynolds stresses measured using acoustic Doppler velocimeters. Values of C_D for the coral substrates ranged from 0.009 to 0.015, three to five times greater than over the sandy bottom site. The turbulence dissipation rate, ε, was determined by fitting spectra of vertical velocity to the theoretical "5/3" law expected for the inertial subrange of turbulence. There was a local balance between production and dissipation of turbulent kinetic energy, signifying that we could estimate u_* from either the mean velocity profile, turbulence, or dissipation rate of turbulent kinetic energy. Estimates from all three measures agreed well with mean u_*/U_o ranging from 0.10 ± 0.03 to 0.12 ± 0.03, indicating that existing turbulent boundary layer flow theory can be applied to flows over the rough topography of coral reefs. The bottom topography, by enhancing both reef scale and local drag and mixing levels, allows reef biota to more effectively exchange dissolved and particulate matter with oceanic waters.

Many coral-reef organisms have limited or no mobility and thus depend on water motion for their basic functions, including food delivery (Kiflawi and Genin 1997; Sebens et al. 1997), production (Koehl and Alberte 1988; Denisson and Barnes 1988), respiration (Goldshmid et al. 2004), uptake of nutrients (Patterson et al. 1991; Atkinson et al. 2001), and larval dispersal (Harii and Kayanne 2003; Sponaugle et al. 2005). The relevant hydrodynamics range from large-scale circulation patterns that determine rates of dispersal across the reef (Hamner and Wolanksi 1988) through microscale turbulence, e.g., motions with length scales near the Kolmogorov scale (Tennekes and Lumley 1972), that influence particle capture and mass flux on the scale of an individual coral polyp (Sebens 1997; Helmuth et al. 1997). The link between these scales is the bottom friction, i.e., shear stresses that develop because of flow over the reef. At intermediate scales of water motion over centimeters to meters, dispersal processes and food acquisition depend on how near-bed flow dynamics exchange mass between the reef and the surrounding ocean. For example, the boundary layer within a few meters of the reef is sometimes severely depleted of planktonic food (Yahel et al. 1998, 2005) because of grazing by the reef community. Replenishment of these food sources depends upon turbulent mixing near the reef (Genin et al. 2002).

Although local, instantaneous turbulent events are important to benthic communities (Abelson and Denny 1997; Crimaldi et al. 2002), the temporally and spatially integrated structure of the boundary layer often best describes relations between flow and transport processes. For instance, it has been shown that the uptake of nutrients by reefs is proportional to the friction velocity, u_* (Baird and Atkinson 1997; Falter et al. 2004). In the same way, it is known that turbulent mixing, represented by the near-bed eddy diffusivity, plays a key role in determining the strength of concentration boundary layers that develop because of benthic grazing (O'Riordan et al. 1993). The average bed stress also plays a critical role in controlling exchange between the reef and the open ocean (Hearn 1999; Monismith et al. 2006). Therefore, an understanding of the structure and dynamics of boundary layer flows and how it relates to smaller- and larger-scale flow phenomena offers valuable insight into the functioning of coral reefs.

[1] Present address: Department of Integrative Biology, University of California, Berkeley, California 94720.

[2] Corresponding author.

[3] Present address: Department of Biology, University of Victoria, P.O. Box 3020 Stn CSC, Victoria, British Columbia, V8W 3N5 Canada.

Acknowledgments

We thank Moty Ohevia, Shiri Eckstein, Ruty Motro, Inbal Ayalon, Eaton Dunkelberger, Roi Holtzman, and Susanne Neilsen for their technical support to the field program and Derek Fong for his assistance in bathymetry mapping.

This work was funded by the National Science Foundation grant OCE 0117859, US-Israel Binational Science Foundation grant 1997450, and the Stanford Bio-X Interdisciplinary Initiatives program. M. Reidenbach was also supported by a Stanford Graduate Fellowship.

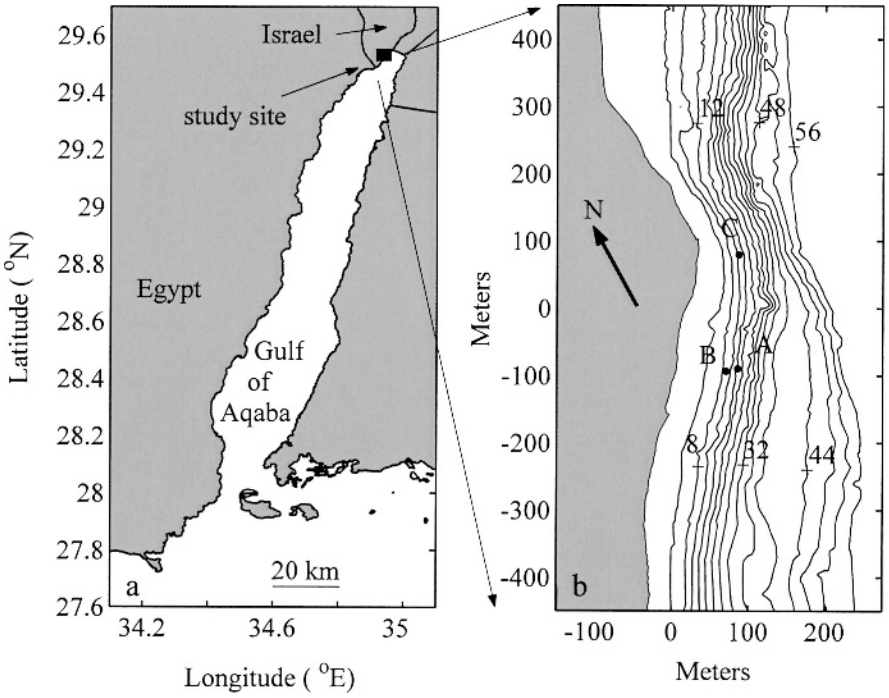

Fig. 1. (a) Site map of the Gulf of Aqaba, with the location of the study area marked with a filled square. (b) Bathymetry map of the three study sites: A, deep coral site (13 m); B, shallow coral site (9 m); and C, sandy bottom site (11 m). Depth contours are in 4-m increments with meter markings shown.

Turbulent boundary layers have been investigated in a variety of coastal environments where the bottom is nearly smooth (Gross and Nowell 1983; Sanford and Lien 1999; Stacey et al. 1999*a*). In these cases, flow structure generally has adhered to the "law of the wall" for turbulent boundary layers, i.e., there is a region near the boundary in which the velocity varies logarithmically and the dissipation of turbulent kinetic energy (TKE), ε, decreases like z^{-1} away from the boundary. Under steady, uniform flow this model can then be used to estimate u_* and the coefficient of drag, C_D (Dewey and Crawford 1988; Kim et al. 2000). From this, parameters such as turbulence length scales and mixing rates can be calculated. These measurements, however, are made under the assumption that there is an equilibrium in which production of TKE, P, is in local balance with ε (Lu et al. 2000). However, direct measurements of both production and dissipation are rare, fairly recent (Krogstad and Antonia 1999; Shaw et al. 2001), and only observed over relatively smooth channel bottoms.

Few studies have looked at flow over extremely rough bottom topographies such as coral reefs. In this environment, assumptions of quasisteady, uniform flow may not hold because the roughness is often patchy, with reef area intermixed with regions of sandy bottom. For example, over a reef system in the Caribbean, Lugo-Fernandez et al. (1998) inferred drag coefficients between 0.06 and 0.2 (see also Hearn 1999). These values are large compared to the canonical value of 0.003 measured over sand or mud bottoms (Heathershaw and Simpson 1978). Whereas this past work suggests that a much higher drag is associated with coral reefs, no detailed studies have been made of how this drag relates to mixing within the benthic boundary layer.

The main goals of this study were therefore (1) to describe the structure of turbulence and flow properties over the reef; (2) to examine whether the turbulent boundary layer obeys the wall-layer scaling, as is found for smoother boundary layers; and (3) to determine rates of production and dissipation of TKE and assess whether the assumption of local equilibrium holds for the reef environment. In pursuing these objectives, key information required for realistic modeling of turbulent flow dynamics in coral reefs was obtained.

Materials and methods

Study site—The experiments were conducted over the fringing coral reefs in the Gulf of Aqaba, Red Sea, between 29 August and 14 September 1999. The study site (Fig. 1), located offshore of the H. Steinitz Marine Biology Laboratory, Eilat Israel, is part of a 5-km stretch of coastline containing reef interspersed with open sand regions devoid of corals. The reef is dominated by hermatypic corals. Soft corals, anemones, sponges, tunicates, and polychaetes are also common (Yahel et al. 2002 and references therein). The fringing reef begins at a water depth just below the mean low tide mark, extending to 80-m depth, although some corals are found as deep as 150 m (Fricke and Schuhmacher 1983). The average slope of the bathymetry between 0 m and 50 m is 24°, with two mildly

Fig. 2. (a) Coral site A with an acoustic doppler current profiler in the foreground and the acoustic Doppler velocimeters array in the background, (b) site A with plastic sheeting covering the bottom topography, and (c) sandy Bottom site C.

sloped terraces at depths of 8 m and 24 m. The percent cover of live corals during the time of this study was 14%; rocky substratum, 29%; and sandy substrate, 57%.

Two sections of the coral reef (A and B in Fig. 1b) and a single sandy site (C in Fig 1b) were selected for the experiment. The two coral sites were at mean depths of 13 m and 9 m, where the bottom slopes were 27° and 18°, respectively, whereas the sandy site was at 11-m depth with a bottom slope of 24°. Roughness transects were conducted over the reef sites to determine the typical topographic roughness height of the coral community. Approximate roughness lengths were measured by stretching a taught line connected to two buoys across 15 m in the along-shore direction of the test section. The line was positioned 1 m above the mean bed height, and the roughness was estimated by measuring the vertical distance, to the nearest half centimeter, between the line and the highest point of relief. These measurements were repeated at 0.5-m increments along the line. Five transects moving from onshore to offshore were completed, which gave roughly 150 measurements at each site. For both coral sites, the mean height of the roughness was 20 cm with a standard deviation of 16 cm. Measurements at the sandy site were not taken, but roughness elements (primarily gravel and small rocks) were visually estimated to be 2–3 cm. This site was located in the middle of an approximately 100-m long section of a smooth, sandy, and loose-gravel bottom with rare occurrence of corals (<1% cover). To further evaluate the contribution of small-scale roughness to the development of flow and turbulence characteristics and to serve as a biological control for grazing in a companion study (Genin et al. 2002), clear plastic sheeting was suspended just above a 20 × 10 m area of the reef at site A. This sheeting effectively smoothed the roughness of individual coral colonies while retaining the general shape of knolls, clumps of corals, and the rocky substrate (Fig. 2). All sites were <75 m offshore, which enabled instruments to be cabled directly to computers within the laboratory, located 25 m from the shoreline.

The 17-day-long summer experiment began just as air and water temperatures started to decline, following a peak in air temperatures of > 44°C. Water temperature steadily decreased from 28°C at the start of the experiment to 25.5°C at its end, with a concurrent drop in salinity from 40.8 to 40.6 (Fig. 3). Tidal variations in surface-water level were approximately 0.8 m. Winds during the experiment were always to the southwest with a mean velocity fluctuating diurnally between 4 m s^{-1} during the night and 7 m s^{-1} during the day. A common feature of this reef, as is the case in many fringing and lagoonal reefs, was the absence of wave activity. Because of the short fetch between the northern end of the gulf and the study site, surface waves during the experiment were minimal, with wave heights <20 cm. No oscillatory motion was measured at depth at any of the study sites. Daily conductivity and temperature profiles (taken with an Applied Microsystems conductivity, temperature depth [CTD] probe) indicated that the thickness of the upper mixed layer was between 15 m and 25 m. For a few hours during the mid-afternoon, solar heating created a weak, near-surface stratified layer 1–2-m thick, which was mixed out during the cooler nighttime hours (Monismith et al. 2006). Conductivity and temperature profiles showed no measurable stratification between 2 m below the surface layer and the bottom, with the gradient Richardson number well below the critical value of 0.25. Detailed oceanographic conditions of the region are described further in Reiss and Hottinger (1984). Measurements at site A were made during days-of-the-year 238–244 (coinciding with spring tides), at site B during days 244–250 (neap tides), and at the sandy site C during days 250–255 (spring tides). Time is reported as local (GMT + 2 hours).

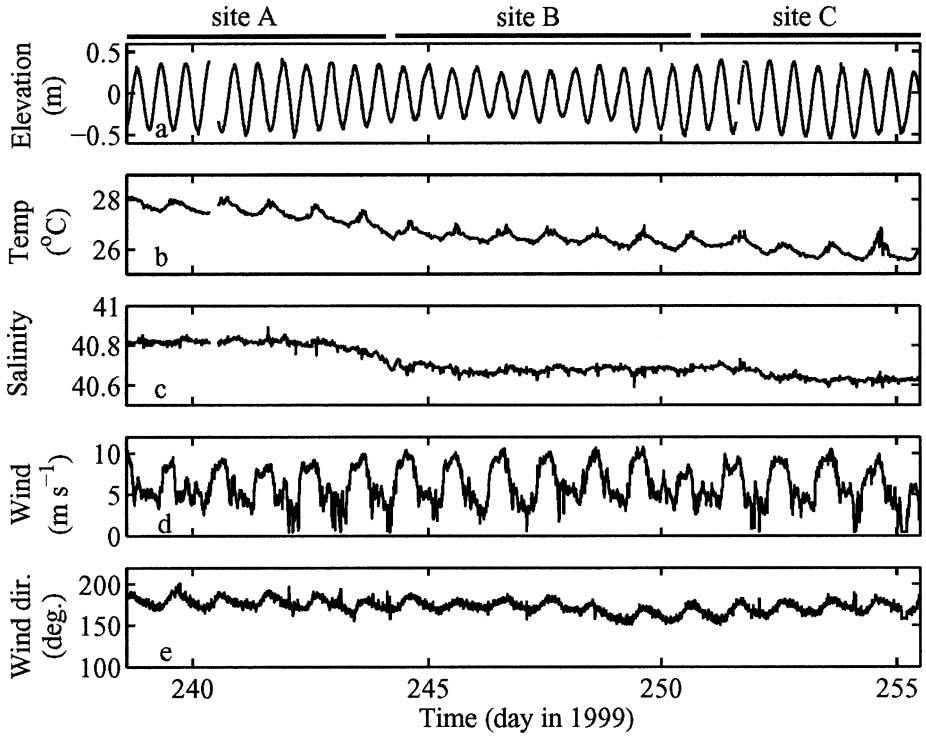

Fig. 3. Time series of (a) sea surface elevation, (b) surface water temperature, (c) salinity, (d) wind magnitude, and (e) wind direction in degrees from true north. All parameters were measured from the laboratory pier, located 100 m to the north of the coral study sites.

Observational setup—Three acoustic Doppler velocimeters ([ADV] 10-MHz Ocean ADV, Sontek Inc.) measured velocities at a rate of 25 Hz at z = 0.1, 0.3, and 1.0 m above the bottom. The ADVs were located within a uniform patch of coral along the center of the reef. Located 5 m from the array was an acoustic Doppler current profiler ([ADCP] WH-600 ADCP, 600 KHz, RDI Inc.) programmed to profile the water column in 0.5-m bins between 1.5 m above bottom and 1 m below the water surface. The ADCP recorded 100-ping velocity ensembles every 40 s, giving a per sample standard error of 1 cm s^{-1}. All instruments were placed as close as possible to one another to ensure they measured the same flow conditions, but were arranged perpendicular to the main axis of flow to minimize flow disturbances by neighboring instruments. Measurements were made relative to datum equal to the local height of the sand bed at the base of the corals. This allowed for consistent measurements between both the coral sites and the sand bottom site and enabled us to determine the relative effect of the coral roughness on the structure of the boundary layer.

Data analysis—Instantaneous velocity measurements were rotated into local bathymetry coordinates of along-shore (U), across-shore (V), and vertical (W) directions. Since most of the water motion was driven by tidal action in the along-shore, this direction (45° from true N during positive flow, 225° during negative flow) was used as the main axis of flow. Mean velocity and turbulence statistics were computed by averaging over 10-min intervals. This time period was chosen because in statistical tests, 10 minutes often emerges as the best balance between obtaining convergence of the mean statistics while minimizing velocity drift caused by changes in tidal flow conditions (i.e., Gross and Nowell 1983). The ADV records were combined with ADCP records to make complete velocity profiles throughout the water column. For the turbulence measurements, which were all measured within 1 m from the bottom, a coordinate system was used in which z is perpendicular to the bottom. Above 1 m, velocity statistics were calculated using a reference frame where z is vertical since it was assumed that flow properties were less influenced by the bottom slope higher within the water column. This change in coordinate system had no effect on the velocity component in the along-shore flow direction and, on average, there was <10% variation in the turbulence measurements ($\overline{u'w'}$) calculated using the two reference frames. The following conventions were used for flow direction: positive along-shore flows correspond to a Northeast-ward (NE) current, whereas negative values correspond to a Southwest-ward (SW) current. Positive across-shore flow is offshore (to the Southeast at 135°), and positive vertical velocities represent upwelling.

Bottom shear stress, $\tau_o = \rho u_*^2$ (where ρ is the density of the fluid) is arguably the single-most important boundary layer parameter because it is a measure of the frictional interaction between the flow and the bottom. However, direct measurements are difficult in the field because of complex bed geometries. Instead, mean flow and turbu-

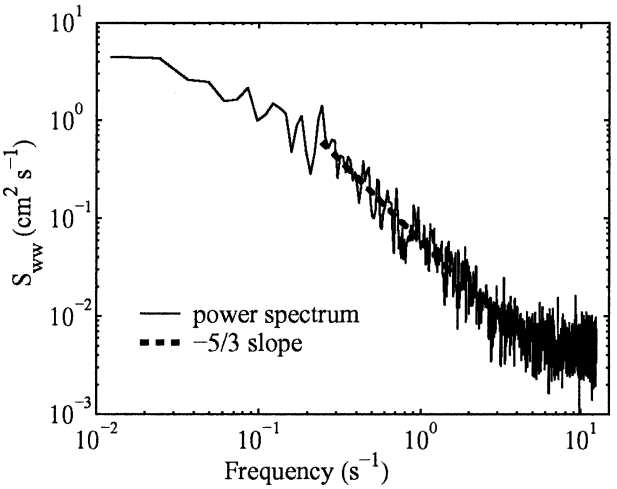

Fig. 4. Typical power spectrum using the vertical velocity component at z = 1 m (site B). The ADV noise floor is 0.005 cm^2 s^{-1}. Note no existence of measurable wave energy within the spectrum.

lence measurements were obtained higher in the water column, and these values were used to infer stresses imposed at the bed. Three common techniques were used to estimate u_*: (1) the logarithmic law, (2) the covariance, and (3) the dissipation technique.

Logarithmic law technique: For a well developed turbulent boundary layer, an inertial sublayer region exists where mean velocities exhibit a logarithmic profile. Within this region, the mean velocity profile is related to the generation of turbulence by shear at the bed, and the law of the wall takes the form (Kundu 1990):

$$U(z,t) = \left(\frac{u_*(t)}{\kappa}\right) \ln\left(\frac{z-d}{z_o}\right) \tag{1}$$

where $\kappa = 0.41$ is von Karman's constant, d is the displacement height, and z_o is the bottom roughness length scale. Values of u_*, d, and z_o were adjusted to obtain a best fit, in the least squares sense, through the logarithm of mean velocities. Eight measurement points were used in the fit, three from ADV measurements between 0.1 m and 1 m above bottom and five from ADCP measurements between 1.5 m and 3.5 m above bottom. Above this, a deviation from a logarithmic profile occurred because of wind stress at the surface. At each site, it was assumed that both d and z_o are properties of the bed roughness and independent of time, which is valid for the timescales of the experiment (Cheng et al. 1999; Stacey et al. 1999*b*). To ensure a well defined log region over the measurement points used in the fit, only profiles having an $r^2 > 0.8$ were used in the analysis. This gives a 95% confidence interval for u_* of ± 28% (Drake et al. 1992).

Covariance technique: The estimation of u_* through the covariance technique assumes that Reynolds stresses are constant within the inertial sublayer (Tennekes and Lumley 1972) and outside of this region linearly decrease to zero at the outer edge of the boundary layer. Within the constant stress region, Reynolds stresses can be used to estimate the friction velocity as

$$u_* = \left|\overline{u'w'}\right|^{\frac{1}{2}} \tag{2}$$

Velocity fluctuations were calculated by subtracting mean velocity values over 10-min intervals from instantaneous measurements $u' = u - U$, $v' = v - V$, $w' = w - W$. Using the three ADVs sampling at 25 Hz, direct calculation of Reynolds stresses were made, and their average stress was used in Eq. 2.

Dissipation technique: The rate P at which energy is produced from mean flow into TKE is estimated as the product of the Reynolds stress times the mean shear:

$$P = -\overline{u'w'}\frac{\partial U}{\partial z} - \overline{v'w'}\frac{\partial V}{\partial z} \tag{3}$$

If a balance between P and the rate of TKE dissipation (ε) occurs where $P = \varepsilon$, the law of the wall in the constant stress region can be used to relate the friction velocity to the dissipation rate as $\frac{u_*^3}{\kappa z} = \varepsilon$ (Dewey and Crawford 1988). Dissipation itself can be calculated independently through spectral measurements of velocity fluctuations and an equation for the friction velocity can be written as

$$u_* = (\varepsilon \kappa z)^{\frac{1}{3}} \tag{4}$$

Dissipation was estimated from a one-dimensional spectral equation of vertical velocity fluctuations (Shaw et al. 2001):

$$S_{ww}(k) = \frac{9}{55}\left(\frac{4-\cos\theta}{3}\right)\alpha\varepsilon^{\frac{2}{3}}k^{-\frac{5}{3}} \tag{5}$$

where $S_{ww}(k_1)$ is the power spectral density as a function of the wave number k; $\theta = 90^\circ$ is the angle from the direction of mean flow; and $\alpha = 1.56$ is the empirical Kolmogorov constant for velocity. Using Taylor's frozen turbulence hypothesis, wave number space was converted to frequency space as $f = \frac{Uk_1}{2\pi}$. Spectra were formed by averaging 7 independent spectra of 2,048 sample records spanning a 10-min time period (Fig. 4). To determine the location of an inertial subrange, i.e., where spectra show a −5/3 slope, the noise floor of the spectrum was first removed, and a linear regression of $\log(S_{ww})$ versus $\log(f)$ was carried out over $n = 148$ points (spanning 0.8 decades). ε was then estimated through Eq. 5 by determining the spectral intensity $[f_1, S_{ww}(f_1)]$ within the inertial subrange, giving 95% confidence of ± 0.13ε. Most of the uncertainty in ε is in estimating the magnitude of the power spectrum at a given frequency (Gross and Nowell 1985). To ensure a full separation of scales, a minimum shear Reynolds number, $Re_* = \frac{u_*\kappa z}{\nu}$ criterion was applied to the data (Gross and Nowell 1985). Although there is no universal value of Re_* above which a well defined inertial subrange exists, our

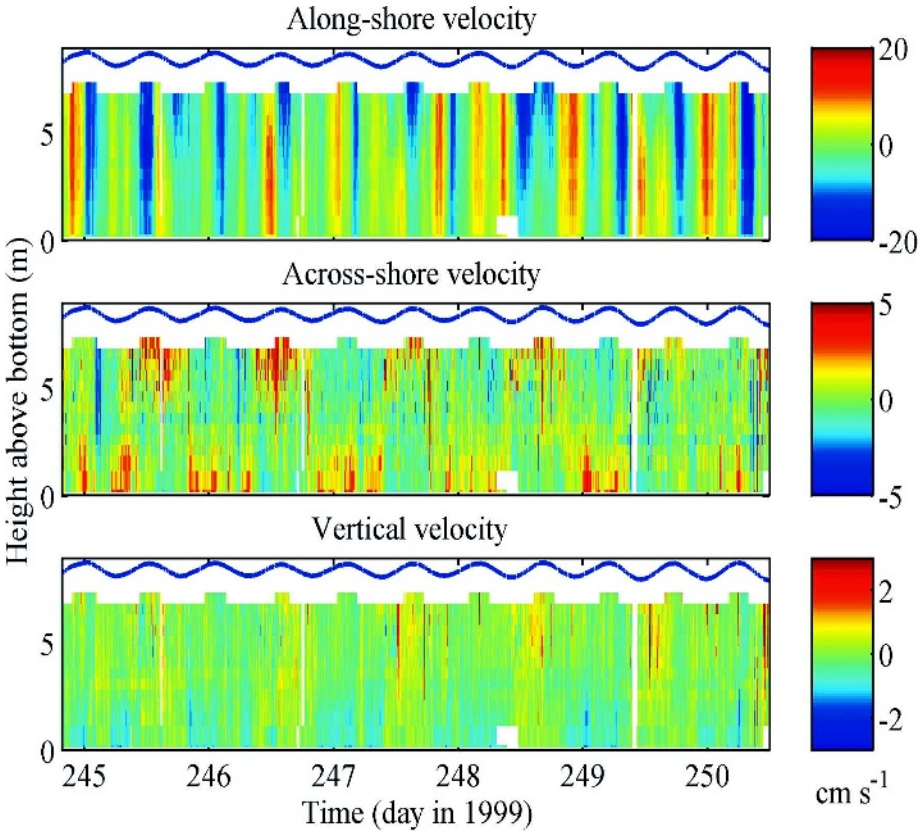

Fig. 5. Combined ADCP and ADV mean velocities at site B in the along-shore, across-shore, and vertical directions. The ADVs were turned off between days 248.3 to 248.5 to backup the data, therefore there is no flow information for this time period within 1 m from the bottom.

data showed that a definitive $-5/3$ slope region existed in spectra when $u_* > 0.4$ cm s^{-1}. This criteria gives a minimum $Re_* = 2{,}000$ at $z = 1$ m, similar to the criteria of $Re_* = 2{,}500$ found by Huntley (1988).

Results

Mean currents and Reynolds stresses—Flows along the reef were primarily driven by semidiurnal internal tides (Monismith and Genin 2004). Mean currents at the coral sites were 5 cm s^{-1} with peak flows on the order of 20 cm s^{-1} (Fig. 5). Velocity profiles as well as daily CTD profiles indicated that the bottom boundary layer had a thickness of 5 m to 7 m and was not influenced by stratification at the study sites. Because of a wind stress imposed at the surface, there was often a surface boundary layer that blended in with the bottom boundary layer at mid-water column. This caused the bottom boundary layer to deviate from a logarithmic profile starting at a height of 3.5 m to 5 m above the bed. Overall, the wind-driven flow led to stronger currents to the SW than to the NE. As described in Monismith et al. (2006), at all sites there were across-shore flows associated with diurnal cooling and heating of waters over the reef (Fig. 5b).

The alongshore Reynolds stress tensor, i.e., $\overline{u'w'}$, and the TKE, $q^2 = \frac{1}{2}\left(\overline{u'u'} + \overline{v'v'} + \overline{w'w'}\right)$, for all sites are shown in Fig. 6. The Reynolds stress ($\overline{u'w'}$) exhibited expected boundary layer characteristics, with values at the three ADV measurement heights being roughly equal. This agreement suggests the existence of a constant stress region within the near-bed turbulent boundary layer. TKE at all the sites decreased with increasing height from the bed. Mean estimates of $-\overline{u'w'}/q^2$, which is the amount of frictional energy imparted at the boundary due to TKE, were 0.12, 0.11, and 0.11 ($\pm$0.02) at coral sites A and B and sand site C, respectively. These values are consistent with estimates found in other tidally dominated flows of 0.08 (Lu et al. 2000) and 0.14 (Gross and Nowell 1983).

Between days 242.5 and 244.5, the plastic sheeting placed over a 20 m $\times$ 10 m section of reef at site A removed the fine-scale relief and small-scale roughness of the coral benthic community. Nonetheless, there was no statistical difference in measured turbulence levels with and without the sheeting in place (site averaged $\left|\overline{u'w'}\right| = 0.59 \pm 0.14$ cm^2 s^{-2} without cover and 0.52 ± 0.12 cm^2 s^{-2} with cover). Even 10 cm above the bed, the integrated effect of the underlying reef topography appears to determine turbulence statistics, not the drag of individual coral heads

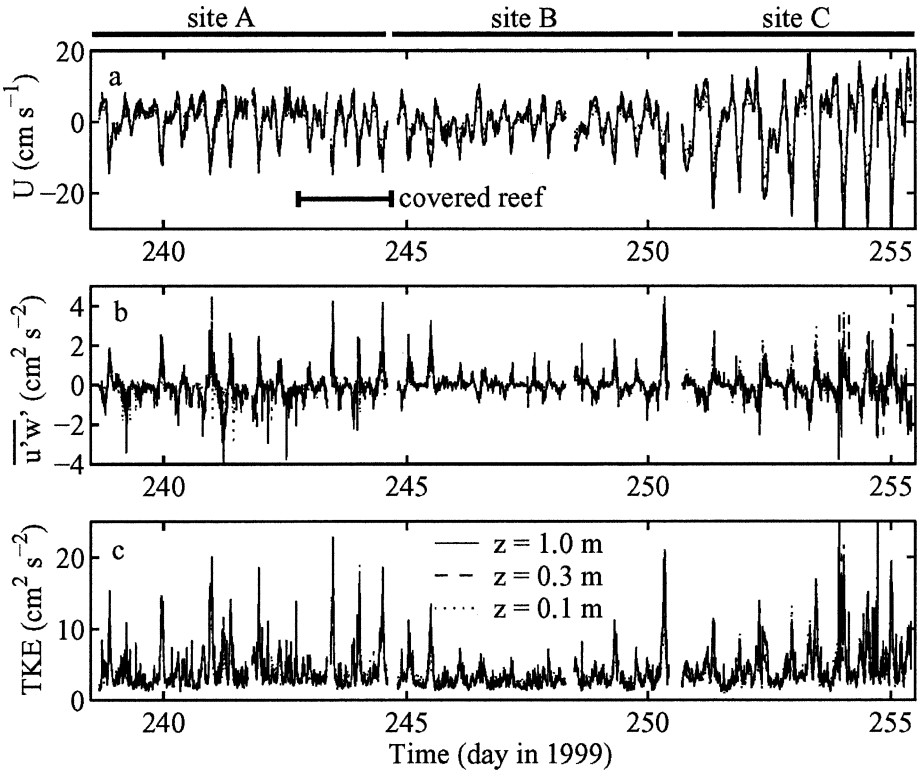

Fig. 6. (a) Mean velocities, (b) Reynolds stresses, and (c) TKE for z = 1 m, 0.3 m, and 0.1 m for sites A, B, and C. The time period during which site A was covered with plastic sheeting is marked in (a).

or the localized friction around the coral fine-scale branching structure.

Production and dissipation of turbulent kinetic energy—TKE production estimates were obtained as the product of the ADV-derived Reynolds stresses and the local velocity gradients at the ADV heights, obtained from logarithmic fits to the mean velocity profile. Figure 7 shows the comparison between production and dissipation estimates at z = 0.1 m, 0.3 m, and 1.0 m for coral sites A and B and the sand site C. The plots indicate variability during weak flow conditions, but values of production and dissipation converge at higher intensities (r^2 for the P = ε fit at z = 1.0 m, 0.3 m, and 0.1 m are site A, 0.54, 0.55, 0.60; site B, 0.69, 0.84, 0.71; and site C, 0.54, 0.73, 0.82; respectively). Most of the observed ε values lie between 10^{-3} and 1 cm^2 s^{-3} (equivalent to 10^{-7} and 10^{-4} W kg^{-1}). Systematic differences in production and dissipation levels occurred at values below 10^{-2} cm^2 s^{-3}, suggesting a noise floor for P and ε estimates.

As the strength of the mean flow increases, production and dissipation levels also increase and a local production–dissipation balance is evident. This is consistent with expectations for unstratified near-wall regions in a turbulent boundary layer. During periods of high flow, near-bed maximum P and ε rates were of similar magnitude at both the coral and sand sites, i.e., on the order of 1 cm^2 s^{-3}. Given that peak velocities at the coral sites were half those at the sand site, it is clear that the flow over the reef is substantially more turbulent at a given velocity than flow over the sandy bed, i.e., it has relatively higher dissipation rates and turbulence intensities than does the sandy site.

TKE production decayed away from the boundary, and to a first approximation, follows the relation P $\sim$ 1/z that is expected from the law of the wall. Dissipation profiles also exhibited this trend, especially during high flow periods when a well defined inertial range existed. This balance also signifies that non-local vertical transport of TKE, which often occurs within the wakes of blunt bodies and causes an imbalance between P and ε (Finnigan 2000), was negligible. Measurements of turbulent transport (calculated as $\frac{\partial \overline{q'^2 w'}}{\partial z}$) within 1 m of the reef was generally on the order of 10^{-4} cm^2 s^{-3}, which was 10^2–10^4 times lower than local production rates.

Roughness length scales and friction velocities—Using a least-squares regression, values of the displacement heights converged to d = 0.06 $\pm$ 0.02 m for each of the coral sites and d = 0.02 $\pm$ 0.005 m for the sand site. Fixed values of z_o, termed $z_{o\text{-global}}$, were calculated as the log-average of the individual 10-min estimates of z_o (i.e., $z_{o-global} = \exp\langle \ln(z_0) \rangle$). Variations in $z_{o\text{-global}}$ estimates were found depending on the site and direction of flow, presumably because of differences in upstream topography. Therefore, separate estimates were formed for both NE and SW flow conditions (Table 1). This within-site variability was not unexpected because of the many length scales that

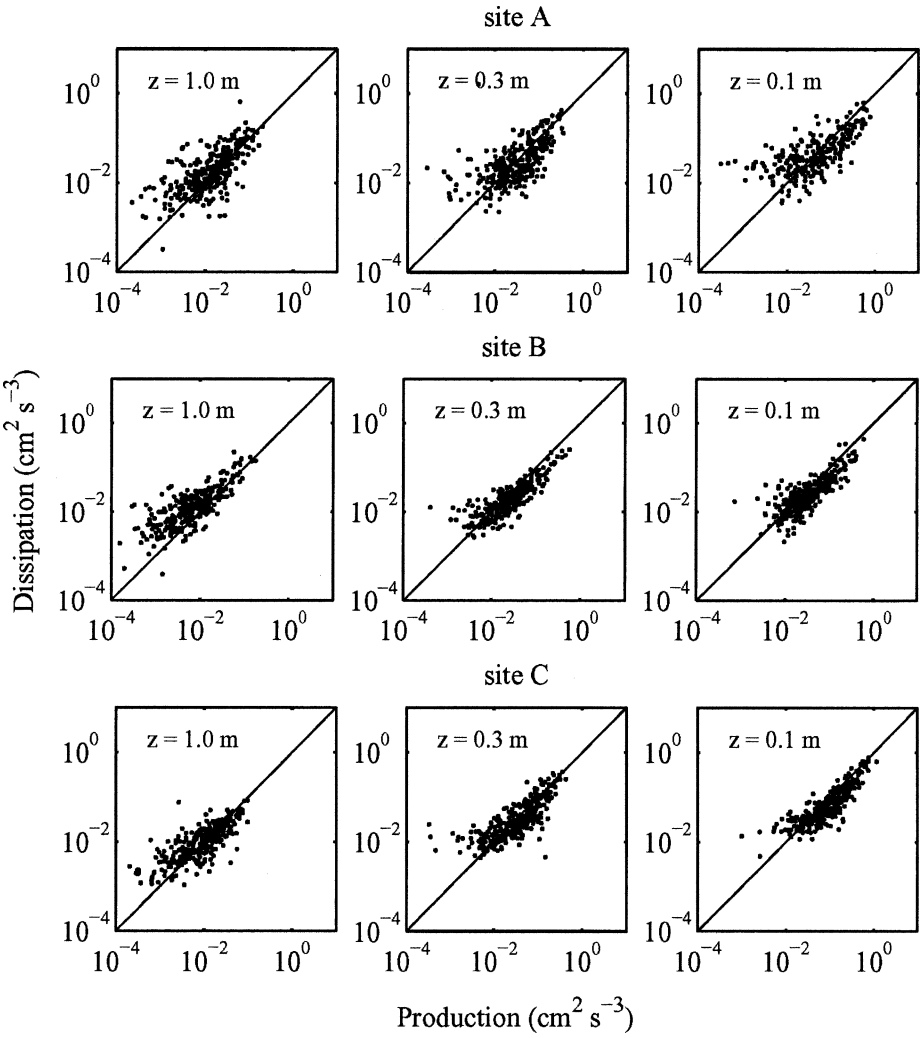

Fig. 7. Production versus dissipation at the three ADV locations z = 1.0 m, 0.3 m, and 0.1 m, respectively.

Table 1. Global roughness lengths for flows to the NE and SW. Uncertainties are reported as 95% confidence on the mean.

Site	NE $z_{o\text{-}global}$ (cm)	SW $z_{o\text{-}global}$ (cm)
A	1.3±0.2	1.0±0.2
B	1.9±0.2	3.9±0.3
C	0.4±0.1	0.1±0.1

exist within the reef, including the size of the coral roughness elements, their spacing, and the relative contribution their morphology plays in generating drag. Values for the coral sites ranged from $z_{o\text{-}global}$= 1.0–3.9 cm, compared to 0.1–0.4 cm for the sand site. This 10-fold increase in roughness length is because of the large effect that the coral has on the flow.

Using measured values of d and $z_{o\text{-}global}$, friction velocities were estimated using the log-law technique and compared to estimates obtained from the covariance and dissipation techniques (Fig. 8). In general, there is very good agreement between the techniques, and a linear relation was found between u_* and U_o for all the estimates. This is indicative of the interdependence of turbulence, velocity shear, and energy levels on mean flow conditions. The log-law technique tends to slightly overpredict u_* compared to the other two techniques (Table 2). The likely cause for this discrepancy is the existence of a pressure gradient that acts to reduce the magnitude of the Reynolds stress away from the bed (Gross and Nowell 1985; Rippeth et al. 2002). Nonetheless, the estimates of u_* from the three techniques agree within 95% confidence intervals. For a given U_o, u_* across the reef sites was consistently double that measured over the sandy bed, with mean u_*/ U_o of 0.12 ± 0.02 and 0.10 ±0 .02 at coral sites A and B, respectively, compared to 0.06 ± 0.01 for the sand site C.

Mixing coefficients and turbulence length scales—Measurements of mean velocity and turbulence parameters enable the calculation of turbulence characteristics that are of particular interest in transport studies: namely, the eddy

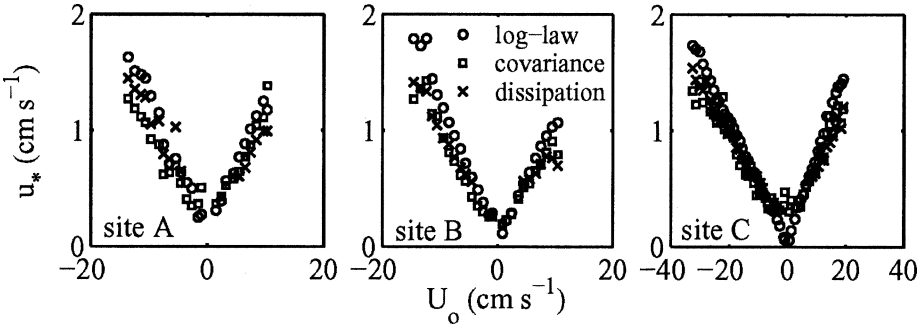

Fig. 8. Comparison of u_* estimates from log-law, covariance, and dissipation techniques for coral site A, coral site B, and sand site C. Each estimate is the binned average over a 1 cm s^{-1} increment of U_o. Note the doubling of the mean velocity scale of plot C compared to A and B, indicating that the relative friction velocity to mean velocity ratio of the coral sites is twice that of the sandy bottom site.

Table 2. Estimates of $\frac{u_*}{U_o}$ by the log-fit, covariance, and dissipation techniques during SW and NE flow conditions.

	Site A		Site B		Site C	
Technique	SW	NE	SW	NE	SW	NE
Log-fit	0.11±0.02	0.12±0.03	0.11±0.02	0.10±0.02	0.06±0.01	0.08±0.01
Covariance	0.10±0.02	0.12±0.03	0.10±0.02	0.10±0.02	0.05±0.01	0.07±0.01
Dissipation	0.12±0.02	0.11±0.02	0.10±0.02	0.10±0.02	0.05±0.01	0.06±0.01

Table 3. Mean eddy viscosity (ν_e) and mixing length (l_m) estimates at the three ADV locations.

Mixing parameter	z (cm)	Site A	Site B	Site C
ν_e (cm^2 s^{-1})	100	35±7	25±5	33±7
	30	11±2	6.5±1.4	11±2
	10	2.3±0.5	2.7±0.6	4.1±0.9
l_m (cm)	100	38±3	39±2	44±2
	30	12.7±0.8	10.6±0.5	14.6±0.6
	10	3.3±0.3	5.2±0.2	5.7±0.2

viscosity, ν_e, and the mixing length, l_m. The eddy viscosity is defined in terms of the mean shear, $S \equiv \frac{\partial U}{\partial z}$ (e.g., Tennekes and Lumley 1972)

$$\nu_e = \frac{-\overline{u'w'}}{\frac{\partial U}{\partial z}} \tag{6}$$

whereas the turbulent mixing length, which is the typical size of a turbulent overturn, is defined as

$$l_m = \frac{\sqrt{-\overline{u'w'}}}{\frac{\partial U}{\partial z}} \tag{7}$$

Values for these two parameters at all three sites are summarized in Table 3. Whereas estimates of ν_e are dependent on the magnitude of the flow, the mixing length scale should be independent of flow rate. Under the formulation of l_m, if the mean shear fits the law of the wall theory, then in unstratified, wall-bounded shear flows the mixing length is proportional to distance from the wall, i.e., $l_m = \kappa z$. At the ADV sampling heights, 100 cm, 30 cm, and 10 cm, this gives a prediction of l_m = 40 cm, 12 cm, and 4 cm, respectively. Our measurements agree with these predicted values and have similar magnitudes both at the coral sites and the sand site. Likewise, using wall scaling in the bottom boundary layer, $\nu_e = u_* \kappa z$. Values of ν_e calculated from Eq. 6 and normalized by $u_* \kappa z$ agree; we find $\nu_e/(u_* \kappa z)$ of 1.01 ± 0.10, 0.93 ± 0.08, and 1.06 ± 0.08 for sites A, B, and C, respectively. This agreement is important because it allows for the estimation of the eddy diffusivity, κ_e, from the law of the wall via the Reynolds analogy ($\nu_e \cong \kappa_e$), and, hence, the computation of the flux of scalars (i.e., plankton, larvae, etc.) from measures of concentration gradients.

Drag coefficient—The coefficient of drag, C_D, is defined as the square of the friction velocity divided by the square of the reference velocity, U_o.

$$C_D \equiv \frac{u_*^2}{U_o^2} \tag{8}$$

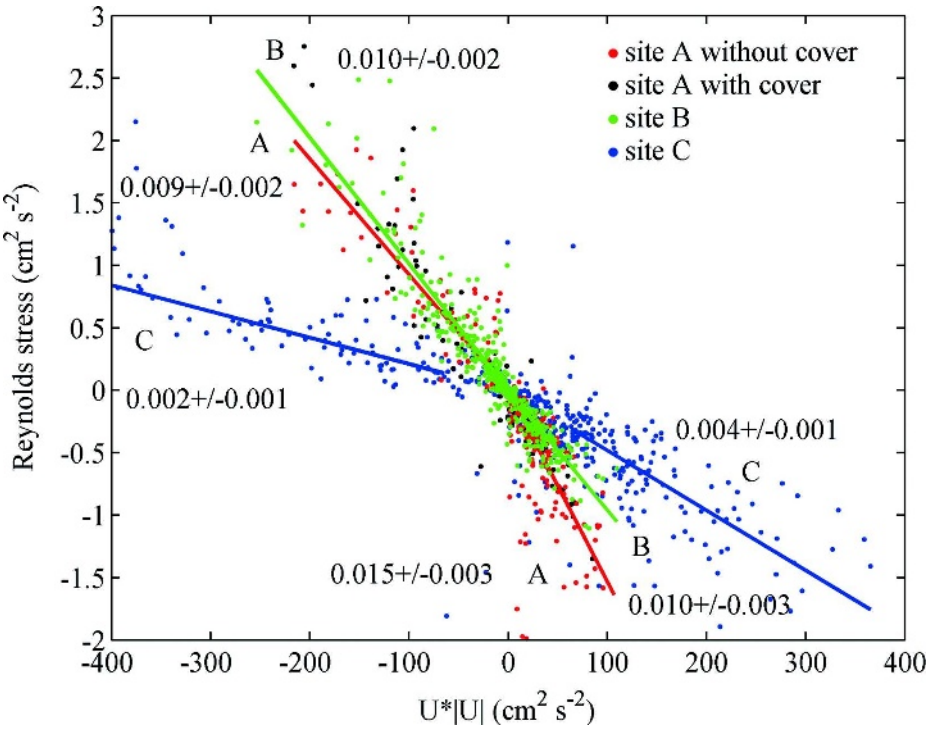

Fig. 9. Along-shore velocity $U_o|U_o|$ versus $\overline{u'w'}$ for sites A (with and without covering), B, and C. The slope of the best fit line, as reported on the graph, corresponds to the coefficient of drag, C_D.

U_o can be defined in a number of ways, but here the reference used is the mean velocity at 1.0 m above the bottom. Using the covariance technique to estimate u_*^2, C_D was calculated as the slope of the best fit line between the square of U_o versus $\overline{u'w'}$ (Fig. 9). Drag values over the coral sites were 3–5 times larger than those estimated at the sand site, characterized by $0.002 \pm 0.001 < C_D < 0.004 \pm 0.001$, depending on flow direction. These measurements are similar to the canonical value of $C_D = 0.003$ used for flows over relatively smooth sand or mud beds. The average drag coefficient across the reef was $C_D = 0.011$, but depending on flow direction, values varied from 0.009 to 0.015. These variations in drag between site and direction of flow are likely caused by the combined effect of differences in upstream topography and changes in water depth because of location and tidal variations.

Drag calculations using u_* estimates from the logarithmic technique give similar, but slightly higher values than those calculated through Reynolds stress estimates (C_D from log-fits of the mean velocity profile ranged from 0.010 to 0.016 over the reef). Both techniques for estimating drag show consistent trends of reef sites having 3–5 times larger drag than sites characterized by sand bed roughness. At site A, both the logarithmic and covariance techniques showed no statistical difference in drag with or without the plastic sheeting in place (with the sheeting, values of $C_D = 0.010 \pm 0.004$ and 0.014 ± 0.002 were measured for SW and NE flows, respectively). This is likely due to the greater relative influence of the integrated upstream roughness rather than the effects of local topography adjacent to the sampling location.

Discussion

Flow characteristics of the reef boundary layer indicate that a local equilibrium exists, where the amount of turbulent energy produced is equal to the amount dissipated. This equilibrium is the foundation upon which the classical law of the wall that describes canonical turbulent boundary layers rests. Were the law of the wall not to hold for flows over the Eilat reef, the three independent techniques used to compute u_* would not agree. The fact that the different approaches give consistent answers allows us to conclude that the reef boundary layer is such a canonical turbulent boundary layer. Thus, even though the topography of the reef is highly variable, even a few tens of centimeters above the reef, the profile of the boundary layer looks similar to that of smoother boundary layers, albeit with much higher levels of shear, turbulence, and mixing. The utility of these measurements is that by from these spatially integrated values of u_* it is possible to estimate other known properties of these boundary layers, e.g., eddy diffusivities that vary linearly with distance from the wall and are proportional to u_*. Practically, it also simplifies matters that log-fits to observed mean velocity profiles, as can be obtained with ADCPs (something that is much easier to do than directly measuring the Reynolds stresses), can be used to compute u_*.

Our measurements indicate that values of z_o are only a few centimeters (between 1.0 cm and 3.9 cm) whereas the height of the coral is much larger. However, there is nothing inconsistent with this finding since z_o is a scaling parameter that represents not just the height of the coral, but the integrated effects of the bed geometry. For example, for sand grains, z_o is 1/30 the sand grain diameter. In our case, this would translate to sand grains that are 0.3–1.2 m, at least comparable to the larger features on the Eilat reef. Additionally, the displacement height of the reef was 6 ± 2 cm in height, much less than the average height of the coral. This indicates there is still substantial flow passing within the reef, which is undoubtedly important for maintaining high rates of exchange of nutrients, larvae, dissolved gases, and other constituents with the overlying water column.

No statistically significant changes in turbulence characteristics were observed following the covering of the reef with the plastic sheet. Not only was the drag comparable, but with the plastic sheet, $z_{o\text{–global}} = 1.3 \pm 0.2$ cm and 0.9 ± 0.1 cm for NE and SW flow directions, respectively. These are statistically similar roughness estimates compared to values without the sheet (as reported in Table 1), suggesting that measures of shear and mixing are less influenced by the local roughness than the integrated effects of topography over a large area. Local reef variability or patchiness on the order of centimeters to meters may therefore have little effect on integrated turbulence and mixing properties. This has important implications to reef-scale modeling efforts; it may be that the larger-scale roughness characteristics set the drag coefficient and mixing parameters, not local roughness elements. However, within close proximity to the bed, the detailed shape of the benthic organisms is likely to play a more important role in small-scale turbulent and diffusive transfer processes, which occur immediately adjacent to the coral surfaces (Reidenbach et al. 2006). Over complex roughness like that of a coral reef, one might expect that shear-layer vortices might predominate, such as have been found for seagrass beds (Cornelisen and Thomas 2004) or even much larger roughness elements, such as buildings (Louka et al. 2000). This suggests that our bulk measures of drag may do well in predicting water column mixing but do not accurately predict small-scale flow patterns along and within the structure of individual corals.

Interestingly, elevated values of C_D measured over the fringing reef are still a factor of 10–100 less than what has been deduced from measurements or calibration of circulation models for flow over coral reefs like those in Kaneohe Bay, Hawaii (Hearn 1999) or St. Croix, U.S. Virgin Islands (Lugo-Fernandez et al. 1998). It seems unlikely that differences in details of the bottom topography between these various reef sites can explain this large difference in inferred values of the drag coefficient, especially given that z_o measured for the Kaneohe reef is smaller than what we find for the Eilat reef (Lowe et al. 2005*a*). The most likely cause for this variation in drag is that the field cases reported above involved flows with energetic surface waves, whereas in the present study waves were insignificant. The presence of waves increases the mean stress (Falter et al. 2005), although how exactly waves affect drag remains uncertain and is worthy of further study, given the importance of waves to many reefs (Lowe et al. 2005*b*). However, our measured values of z_o are quite close to what McDonald et al. (2006) found for a continuous bed of 15-cm high *Porites compressa* heads. In contrast, extrapolating the work of Lowe et al. (2005*b*) with cylinder arrays to the case of arrays of large coral heads, "bommies," that are barely submerged (e.g., as found in the reef lagoons on the north shore of Moorea, French Polynesia), much larger effective drag coefficients than what we find in Eilat might be anticipated for some reefs.

Nonetheless, the relatively high values of measured C_D undoubtedly imply enhanced turbulent mixing. This in turn should increase the ability of the benthic community to graze on phytoplankton (Yahel et al. 1998; Genin et al. 2002) and zooplankton (Yahel et al. 2005; Holzman et al. 2005). The factor of four increase in C_D implies a two-fold increase in rates of mixing, thus enhancing replenishment of planktonic food to the benthic community and possibly increasing food uptake and coral growth rates. Likewise, if the reef's bottom roughness and coral growth are correlated, a positive feedback is expected to occur during the succession of a reef. Initially, when corals are sparse and small, C_D is low and growth is expected to be low (assuming similar levels of competition). At more mature stages of succession, after corals have become more abundant and larger, turbulence-enhanced growth should further augment the bottom roughness. However, factors that preferentially cause mortality of large corals, e.g., coral breakage, may offset this heightened growth, thus maintaining the reef roughness at a quasisteady state.

References

Abelson, A., and M. W. Denny. 1997. Settlement of marine organisms in flow. Ann. Rev. Ecol. Sys. **28:** 317–339.

Atkinson, M. J., J. L. Falter, and C. J. Hearn. 2001. Nutrient dynamics in the Biosphere 2 coral reef mesocosm: Water velocity controls NH4 and PO4 uptake. Coral Reefs **20:** 341–346.

Baird, M. E., and M. Atkinson. 1997. Measurement and prediction of mass transfer to experimental coral reef communities. Limnol. Oceanogr. **42:** 1685–1693.

Cheng, R. T., C. H. Ling, and J. W. Gartner. 1999. Estimates of bottom roughness length and bottom shear stress in South San Francisco Bay, California. J. Geophys. Res. **104:** 7715–7728.

Cornelisen, C. D., and F. I. M. Thomas. 2004. Ammonium and nitrate uptake by leaves of the seagrass Thalassia testudinum: Impact of hydrodynamic regime and epiphyte cover on uptake rates. J. Mar. Sys. **49:** 177–194.

Crimaldi, J. P., J. K. Thompson, J. H. Rosman, R. J. Lowe, and J. R. Koseff. 2002. Hydrodynamics of larval settlement: The influence of turbulent stress events at potential recruitment sites. Limnol. Oceanogr. **47:** 1137–1151.

Dennison, W. C., and D. J. Barnes. 1988. Effect of water motion on coral photosynthesis and calcification. J. Exper. Mar. Biol. Ecol. **115:** 67–77.

Dewey, R. K., and W. R. Crawford. 1988. Bottom stress estimates from vertical dissipation rate profiles on the continental shelf. J. Phys. Oceanogr. **18:** 1167–1177.

Drake, D. E., D. A. Cacchione, and W. D. Grant. 1992. Shear stress and bed roughness estimates for combined wave and current flows over a rippled bed. J. Geophys. Res. **97:** 2319–2326.

Falter, J. L., M. J. Atkinson, and M. A. Merrifield. 2004. Mass-transfer limitation of nutrient uptake by a wave-dominated reef flat community. Limnol. Oceanogr. **49:** 1820–1831.

———, ———, and C. F. M. Coimbra. 2005. Effects of surface roughness and oscillatory flow on the dissolution of plaster forms: Evidence for nutrient mass transfer to coral reef communities. Limnol. Oceanogr. **50:** 246–254.

Finnigan, J. 2000. Turbulence in plant canopies. Ann. Rev. Fluid Mech. **32:** 519–571.

Fricke, H., and H. Schuhmacher. 1983. The depth limits of Red Sea stony corals: An ecophysiological problem (a deep diving survey by submersible). Mar. Ecol. **4:** 163–194.

Genin, A., G. Yahel, M. A. Reidenbach, J. R. Koseff, and S. G. Monismith. 2002. Intense benthic grazing on phytoplankton in coral reefs revealed using the control volume approach. Oceanogr. **15:** 90–96.

Goldshmid, R., R. Holzman, D. Weihs, and A. Genin. 2004. Aeration of corals by sleep-swimming fish. Limnol. Oceanogr. **49:** 1832–1839.

Gross, T. F., and A. R. Nowell. 1983. Mean flow and turbulence scaling in a tidal boundary layer. Cont. Shelf Res. **2:** 109–126.

———, and ———. 1985. Spectral scaling in a tidal boundary layer. J. Phys. Oceanogr. **15:** 496–508.

Hamner, W., and E. Wolanski. 1988. Hydrodynamic forcing functions and biological processes on coral reefs: A status review. Proc. 6th Int. Coral Reef Symp. **1:** 103–113.

Harii, S., and H. Kayanne. 2003. Larval dispersal, recruitment, and adult distribution of the brooding stony octocoral Heliopora coerulea on Ishigaki Island, southwest Japan. Coral Reefs **22:** 188–196.

Hearn, C. J. 1999. Wave-breaking hydrodynamics within coral reef systems and the effect of changing relative sea level. J. Geophys. Res. **104:** 30007–30019.

Heathershaw, A. D., and J. H. Simpson. 1978. The sampling variability of the Reynolds stress and its relation to boundary shear stress and drag coefficient measurements. Estuar. Coast. Shelf Sci. **6:** 263–274.

Helmuth, B. S. T., K. P. Sebens, and T. L. Daniel. 1997. Morphological variation in coral aggregations: Branch spacing and mass flux to coral tissues. J. Exp. Mar. Biol. Ecol. **209:** 233–259.

Holzman, R., M. A. Reidenbach, S. G. Monismith, J. R. Koseff, and A. Genin. 2005. Near-bottom depletion of zooplankton over a coral reef: II. Relationships with zooplankton swimming ability. Coral Reefs **24:** 87–94.

Huntley, D. A. 1988. A modified inertial dissipation method for estimating seabed stresses at low Reynolds numbers, with application to wave-current boundary-layer measurements. J. Phys. Oceanogr. **18:** 339–346.

Kiflawi, M., and A. Genin. 1997. Prey flux manipulation and the feeding rates of reef-dwelling planktivorous fish. Ecology **78:** 1062–1077.

Kim, S. C., C. T. Friedrichs, J. P. Y. Maa, and L. D. Wright. 2000. Estimating bottom stress in tidal boundary layer from acoustic doppler velocimeter data. J. Hydraul. Eng. **126:** 399–406.

Koehl, M. A. R., and R. S. Alberte. 1988. Flow, flapping, and photosynthesis of macroalgae: Functional consequences of undulate blade morphology. Mar. Biol. **99:** 435–444.

Krogstad, P. Å., and R. A. Antonia. 1999. Surface roughness effects in turbulent boundary layers. Exp. Fluids **27:** 450–460.

Kundu, P. 1990. Fluid mechanics. Academic Press.

Louka, P., S. E. Belcher, and R. G. Harrison. 2000. Coupling between air flow in streets and the well-developed boundary layer aloft. Atmos. Environ. **34:** 2613–2621.

Lowe, R. J., J. L. Falter, M. D. Bandet, G. Pawlak, M. J. Atkinson, S. G. Monismith, and J. R. Koseff 2005*a*. Spectral wave dissipation over a barrier reef. J. Geophys. Res. **110**. C04001. [doi:10.1029/2004JC002711]

———, J. R. Koseff, and S. G. Monismith 2005*b*. Oscillatory flow through submerged canopies. Part 1. Velocity structure. J. Geophys. Res. **110**. C10016. [doi:10.1029/2004JC002788]

Lu, Y., R. G. Lueck, and D. Huang. 2000. Turbulence characteristics in a tidal channel. J. Phys. Oceanogr. **30:** 855–867.

Lugo-Fernandez, A., H. H. Roberts, W. J. Wiseman, Jr., and B. L. Carter. 1998. Water Level and currents of tidal and infragravity periods at Tague Reef, St. Croix (USVI). Coral Reefs **17:** 343–349.

McDonald, C. B., J. R. Koseff, and S. G. Monismith. 2006. Effects of the depth to coral height ratio on drag coefficients for unidirectional flow over coral: A reconciliation of current data. Limnol. Oceanogr **51:** 1294–1301.

Monismith, S. G., and A. Genin. 2004. Tides and sea level in the Gulf of Aqaba (Eilat). J. Geophys. Res. **109**. C04015. [doi: 10.1029/2003JC002069]

———, ———, M. A. Reidenbach, G. Yahel, and J. R. Koseff. In press. Thermally driven exchanges between a coral reef and the adjoining ocean. J. Phys. Oceanogr.

O'Riordan, C. A., S. G. Monismith, and J. R. Koseff. 1993. A study of concentration boundary-layer formation over a bed of model bivalves. Limnol. Oceanogr. **38:** 1712–1729.

Patterson, M. R., K. P. Sebens, and R. R. Olson. 1991. In situ measurements of flow effects on primary production and dark respiration in reef corals. Limnol. Oceanogr. **36:** 936–948.

Reidenbach, M. A., J. R. Koseff, S. G. Monismith, J. V. Steinbuck, and A. Genin. 2006. The effects of waves and morphology on mass transfer within branched reef corals. Limnol. Oceanogr. **51:** 1134–1141.

Reiss, Z., and L. Hottinger. 1984. The gulf of Aqaba: Ecological micropaleontology. Springer-Verlag.

Rippeth, T. P., E. Williams, and J. H. Simpson. 2002. Reynolds stress and turbulent energy production in a tidal channel. J. Phys. Oceanogr. **32:** 1242–1251.

Sanford, T. B., and R. C. Lien. 1999. Turbulent properties in a homogeneous tidal bottom boundary layer. J. Geophys. Res. **104:** 1245–1257.

Sebens, K. P. 1997. Adaptive responses to water flow: Morphology, energetics and distribution of reef corals. Proc. 8th Int. Coral Reef Symp. **2:** 1053–1058.

———, J. Witting, and B. Helmuth. 1997. Effects of water flow and branch spacing on particle capture by the reef coral Madracis mirabilis (Duchassaing and Michelotti). J. Exp. Mar. Biol. Ecol. **211:** 1–28.

Shaw, W. J., J. H. Trowbridge, and A. J. Williams III. 2001. Budgets of turbulent kinetic energy and scalar variance in the continental shelf bottom boundary layer. J. Geophys. Res. **106:** 9551–9564.

Sponaugle, S., T. Lee, V. Kourafalou, and D. Pinkard. 2005. Florida Current frontal eddies and the settlement of coral reef fishes. Limnol. Oceanogr. **50:** 1033–1048.

Stacey, M. T., S. G. Monismith, and J. R. Burau. 1999*a*. Observations of turbulence in a partially stratified estuary. J. Phys. Oceanogr. **29:** 1950–1970.

———, ———, and ———. 1999*b*. Measurements of Reynolds stress profiles in unstratified tidal flow. J. Geophys. Res. **104:** 10,933–10,949.

TENNEKES, H., AND J. LUMLEY. 1972. A first course in turbulence. The MIT Press.

YAHEL, G., A. F. POST, K. FABRICIUS, D. MARIE, D. VAULOT, AND A. GENIN. 1998. Phytoplankton distribution and grazing near coral reefs. Limnol. Oceanogr. **43:** 551–563.

YAHEL, R., G. YAHEL, AND A. GENIN. 2002. Daily cycles of suspended sand at coral reefs: A biological control. Limnol. Oceanogr. **47:** 1071–1083.

———, ———, AND ———. 2005. Near-bottom depletion of zooplankton over coral reefs: I: Diurnal dynamics and size distribution. Coral Reefs **24:** 75–85.

Received: 30 August 2005
Accepted: 29 March 2006
Amended: 20 April 2006